Grain boundary transition associated intergranular failure analysis at TMAZ/SZ interface of dissimilar AA7475-AA2198 joints by friction stir welding

Grain boundary transition associated intergranular failure analysis at TMAZ/SZ interface of dissimilar AA7475-AA2198 joints by friction stir welding

Mohammad Reza Jandaghi[1,*], Hesam Pouraliakbar[2], Sun Ig Hong[2], Matteo Pavese[1]

[1]*Department of Applied Science and Technology, Politecnico di Torino, Corso Duca degli Abruzzi 24, 10129 Torino, Italy*

[2]*Department of Materials Science and Engineering, Chungnam National University, Daejeon, 34134, Republic of Korea*

**Corresponding author; E-mail: mohammadreza.jandaghi@polito.it*

Abstract

Post-weld heat-treatment (PWHT) of dissimilar AA7475-AA2198 friction stir welds (FSW) at 560 °C followed by water-quenching since cracks were observed at the TMAZ/SZ interface in retreating AA7475 upon quenching. Microstructural studies revealed that composition difference at high-temperature solution-treatment was the driving force for Cu diffusion from advancing AA2198 through grain boundary liquid-metal thin-films, and caused intergranular segregation of a sufficient amount of Cu-Zn phase. Weld residual stresses, weak interfacial strength, grain boundary transition (premelting), and wetting along with thermal expansion coefficient discrepancies were found to be the associated phenomena in intergranular failure.

Keywords: Friction Stir Welding (FSW); Post-weld heat-treatment (PWHT); Grain boundary transition; Diffusion; Failure; Intergranular segregation.

Introduction

Fabrication of strong and reliable aluminum joints would extend their application in the aerospace and automotive industries [1]. Al-Zn-Mg (AA7XXX) and Al-Cu (AA2XXX) alloys are remarkably attractive materials that could benefit from the high strength-to-weight ratio and precipitation hardening. FSW is a solid-state welding technique in which plasticized sheets being joined are not melted but could experience severe plastic deformation at high-temperatures below their melting point [2]. In this process, the intense material turbulence promoted by a rotating pin could simultaneously exploit the precipitation and grain-refinement [3, 4]. PWHT is a conventional approach to improve the mechanical strength of weldments. Often, joints are subjected to solution-treatment at elevated temperatures (450-600 °C) and subsequent rapid cooling [5]. Ergo, aging at low-temperatures encourages the formation of the new strengthening precipitates/phases.

According to the literature, several PHWT cycles have been introduced to the similar/dissimilar joints of AA2XXX and AA7XXX alloys while microstructural evolution and mechanical properties have been scrutinized [5-7]. In this study, the intergranular failure and its associated phenomena after the solution-treatment cycle were analyzed in the dissimilar AA7475-AA2198 FSWed joints.

Experimental procedure

Full-penetration butt-welds of as-received AA7475-W and AA2198-T3 aluminum sheets (thickness: 3 mm) were fabricated by the FSW process using a thread-free cylindrical H13 steel tool (shoulder diameter: 13.45 mm, pin diameter: 4.7 mm, pin height: 3.16 mm). During FSW, AA7475 and AA2198 were considered as retreating and advancing sheets, respectively. The pin angle, traverse speed, and tool rotation of 2°, 50 mm.min^{-1}, and 830 rpm, were applied, respectively. In PWHT, the weld specimens were isothermally solution-treated at 560 °C for 90 min and then water-quenched. Further analyses and inspections on the microstructure evolution, failure surface, and elemental diffusion were performed by optical (OM) and scanning electron microscopy (SEM) techniques.

Results and discussion

The surface and cross-section microstructures of the FSWed specimens were presented in Fig. 1. As shown, the stir-zone (SZ) in the as-weld sample contained the finest grains and weldment was crack-free. Likewise, the morphology of grains in the top surface and cross-section of the PWHTed joint was demonstrated in Figs. 1(c) and 1(d), respectively. As illustrated, solution-treatment caused abnormal grain growth within the SZ and thermo-mechanically affected zone (TMAZ) of AA7475 while this was accompanied by a significant reduction in grain boundary (GB) density. Furthermore, a considerable amount of cracks with the connected pattern emerged after PWHT at the TMAZ/SZ interface of AA7475. The possibility of abnormal grain coarsening while PWHT was reported in earlier studies [2, 8]. The microstructure of the cracked region was inspected by SEM (Fig. 2). According to Fig 2(a, b), individual GB cracks were connected at the SZ boundary and weakened the TMAZ/SZ interface since cracks were not propagated into the SZ. However, grain growth and grains' elongated geometry in TMAZ facilitated cracks' connection. From Fig. 2(c, d) micrographs, it was observed that the GBs in AA7475-TMAZ were wetted by a segregated phase that induced the intergranular failure. As inspected, the cracks propagation/formation path was just along the GBs. According to the literature [7, 9], heat-treatment of Al-Zn-Mg alloys around 480 °C causes premelting while above 565 °C it could lead to complete melting/wetting of the GBs. In the case that GB energy is greater than twice for the solid/liquid energy at a specific temperature, liquid-metal films will be substituted to the GBs and wetting will be progressed to reduce the system energy [7]. The possibility of GB transition was reported for Al-Zn and Al-Mg alloys [2, 7]. Further, the change in GB energy by misorientation alteration in TMAZ would diminish the GB transition temperature. Elemental mapping for the segregated phase in AA7475-TMAZ indicated that the GB phase enriched in Cu and Zn. Comparison of results in Fig. 2(e) and Fig. 3(a) revealed the concurrent diffusion of Cu and Zn occurred at high-temperature treatment from parent metals. At 560 °C in which GB premelting occurred, Cu and Zn solubility in the molten phase were enhanced and Cu diffused through liquid-metal thin-films acted as diffusion guide-channels to wet the GBs. The reduced GB density due to grain growth in TMAZ and the considerable Cu concentration difference between AA7475 and AA2198 was the driving force for the atomic-scale diffusion. The formation of Cu-rich particles in the SZ near the AA7475-TMAZ confirmed the provision of Cu by diffusion since the employed AA7475 sheet did not contain such particles (Fig. 3(b)). According to the Al-Cu-Zn ternary phase diagram and considering the examined chemical compositions (Fig. S1), concurrent Cu and Zn diffusion over 550 °C could lead the formation of Cu-Zn-rich β-phase [10, 11] which can reduce the ductility [12]. Microscopy inspection of the failure surface (Fig. 4) disclosed the formation of the globular structure of aluminum grains and GB precipitates with typical hypereutectic morphology (Fig. S2). The emergence of the spherical/semi-spherical grains within the microstructure confirmed that the solution-treatment temperature and preservation time was adequate to melt the GBs and put the aluminum alloy within the mushy (semi-solid) region. From the micrographs, the GB phase content was approximately 10 vol%. However, this was in good agreement with the derived fractions in a recent study [13]. Such a phase content considering the low amount of Cu in AA7475 composition supported the hypothesis of considerable diffusion through GBs. However, the control of semi-solid temperature in wrought alloys would be effortful due to their wide solidification range [13]. The globular structure was reported for semi-solid temperature (processing) of AA7XXX alloys and it was claimed that the formation of such morphologies along with GB enrichment and subsequent intergranular precipitates could exacerbate the mechanical properties and corrosion resistance via GB weakening/embrittlement especially in precipitation-hardenable alloys [13, 14]. From Fig. 4, the continuous wetting and coverage of GBs and triple junctions by a Cu-Zn phase were evident. It was also inferred that the grain coarsening and phase separation competed while PHWT. Moreover, the absence of dimple structure (ductile rupture) demonstrated that the failure mechanism was GB detachment/debonding due to low adhesion bonding strength of segregated phase and matrix grains. The material in TMAZ experiences a lesser amount of strain compared to the SZ and due to the shape of elongated and bent grains adjacent to SZ, a considerable amount of welding residual stress could be generated while thermal cooling (Fig. S3) [15]. Such stress localization induced a steep stored energy gradient between AA2198 and AA7475. Besides, the discrepancies in the thermal expansion coefficients of the aluminum grains and GB phase and weak adhesion between the grains and Cu-Zn phase, water-quenching imposed intense thermal stresses which eventuated in the failure of the weld samples.

Conclusion

FSWed AA7475-AA2198 aluminum sheets were PWHTed at 560 °C for 90 min since cracks were emerged at TMAZ/SZ interface in retreating AA7475 upon water-quenching. Microstructural studies revealed the formation of the globular aluminum grains due to the GB transition and sufficient amount of the Cu-Zn phase that completely wetted and surrounded the matrix grains. Intergranular Cu-Zn phase segregated due to concurrent diffusion of Zn from AA7475 and Cu from advancing AA2198 via liquid-metal thin-films by concentration difference which was the driving force for atomic-scale diffusion at high-temperature solution-treatment. The phenomena including remarkable welding residual stresses besides geometry of the elongated grains at AA7475-TMAZ, weak interfacial adhesion of aluminum grains and segregated phase, GB premelting and their wetting by intergranular phase as well as the difference in the thermal expansion coefficients of the aluminum and GB phase had a synergetic contribution on the failure of dissimilar FSWed butt-joints due to development of thermal stresses by water-quenching.

References

[1] M.K.G. Shiran, G. Khalaj, H. Pouraliakbar, M.R. Jandaghi, A.S. Dehnavi, H. Bakhtiari, Journal of Manufacturing Processes, 35 (2018) 657-663.

[2] A. Azadi Chegeni, P. Kapranos, Metals, 8 (2018) 41.

[3] H. Shirazi, S. Kheirandish, H. Pouraliakbar, Theoretical and Applied Fracture Mechanics, 105 (2020) 102423.

[4] S. Pasebani, I. Charit, R.S. Mishra, Materials Letters, 160 (2015) 64-67.

[5] H. Sidhar, R.S. Mishra, A.P. Reynolds, J.A. Baumann, Journal of Alloys and Compounds, 722 (2017) 330-338.

[6] M. Jandaghi, C. Badini, M. Pavese, Journal of Manufacturing Processes, 57 (2020) 712-724.

[7] B. Straumal, O. Kogtenkova, P. Zięba, Acta materialia, 56 (2008) 925-933.

[8] I Charit, R.S. Mishra, Scripta Materialia, 58 (2008) 367-371.

[9] E. Rabkin, L.S. Shvindlerman, B.B. Straumal, International Journal of Modern Physics B, 5 (1991) 2989-3028.

[10] B. Malard, F. De Geuser, A. Deschamps, Acta Materialia, 101 (2015) 90-100.

[11] Z. Stošić, D. Manasijević, L. Balanović, T. Holjevac-Grgurić, U. Stamenković, M. Premović, D. Minić, M. Gorgievski, R. Todorović, Materials Research, 20 (2017) 1425-1431.

[12] H. Hong, Q. Wang, C. Dong, P.K. Liaw, Scientific Reports, 4 (2014) 1-4.

[13] B. Binesh, M. Aghaie-Khafri, Metals 6 (2016) 42.

[14] A. Ghosh, M. Ghosh, A.H. Seikh, N.H. Alharthic, Journal of Materials Research and Technology, 9(1) (2020) 1-12.

[15] J.-Q. Su, T. Nelson, R. Mishra, M. Mahoney, Acta Materialia, 51 (2003) 713-729.

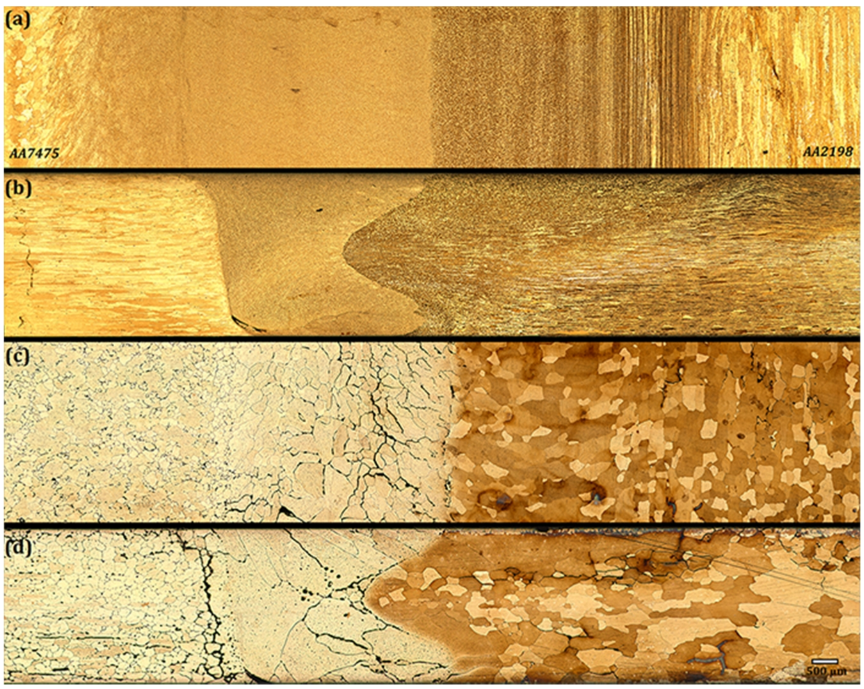

Fig. 1: OM images showing the top surface and cross-section of (a, b) as-weld, and (c, d) solution-treated FSWed specimens, respectively.

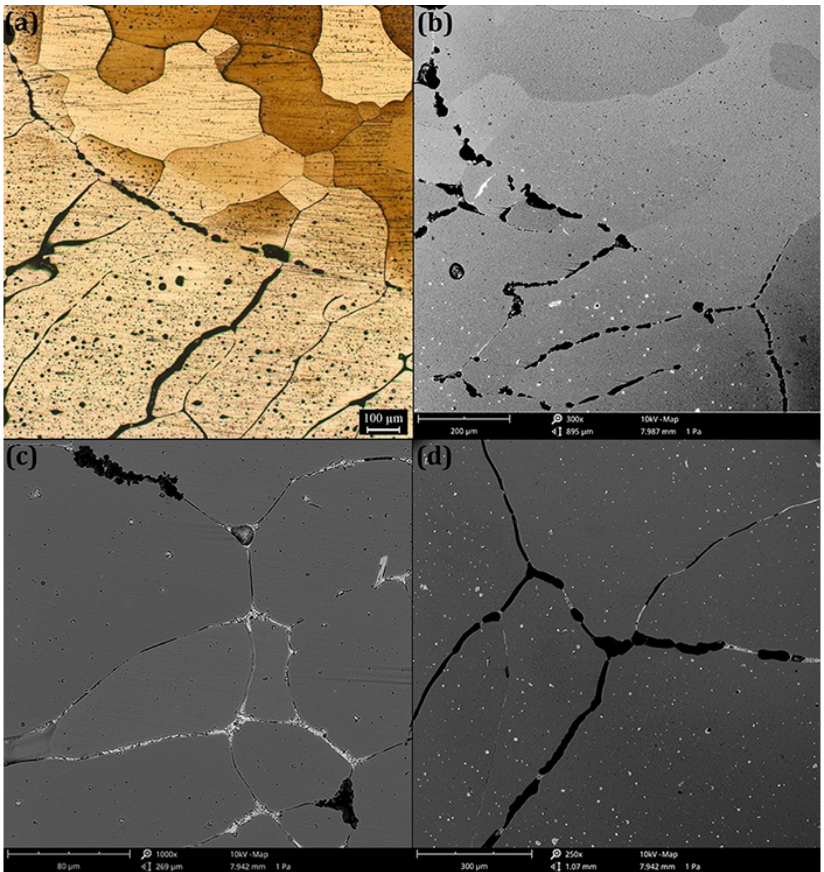

(e)

Element/zone	AA7475	Stir Zone	AA2198
Al (At. %)	93.28	92.79	97.95
Zn (At. %)	2.97	2.9	0
Cu (At. %)	0.75	1.7	2.05
Mg (At. %)	2.7	1.57	0
Fe (At. %)	0.03	0.03	0

Fig. 2: (a) OM and (b) SEM micrographs of the TMAZ/SZ interface, (c, d) BSE-SEM images of the GBs having segregated Cu-Zn phase in AA7475-TMAZ after solution-treatment, and (e) EDS-SEM microchemical analysis obtained for parent metals and SZ.

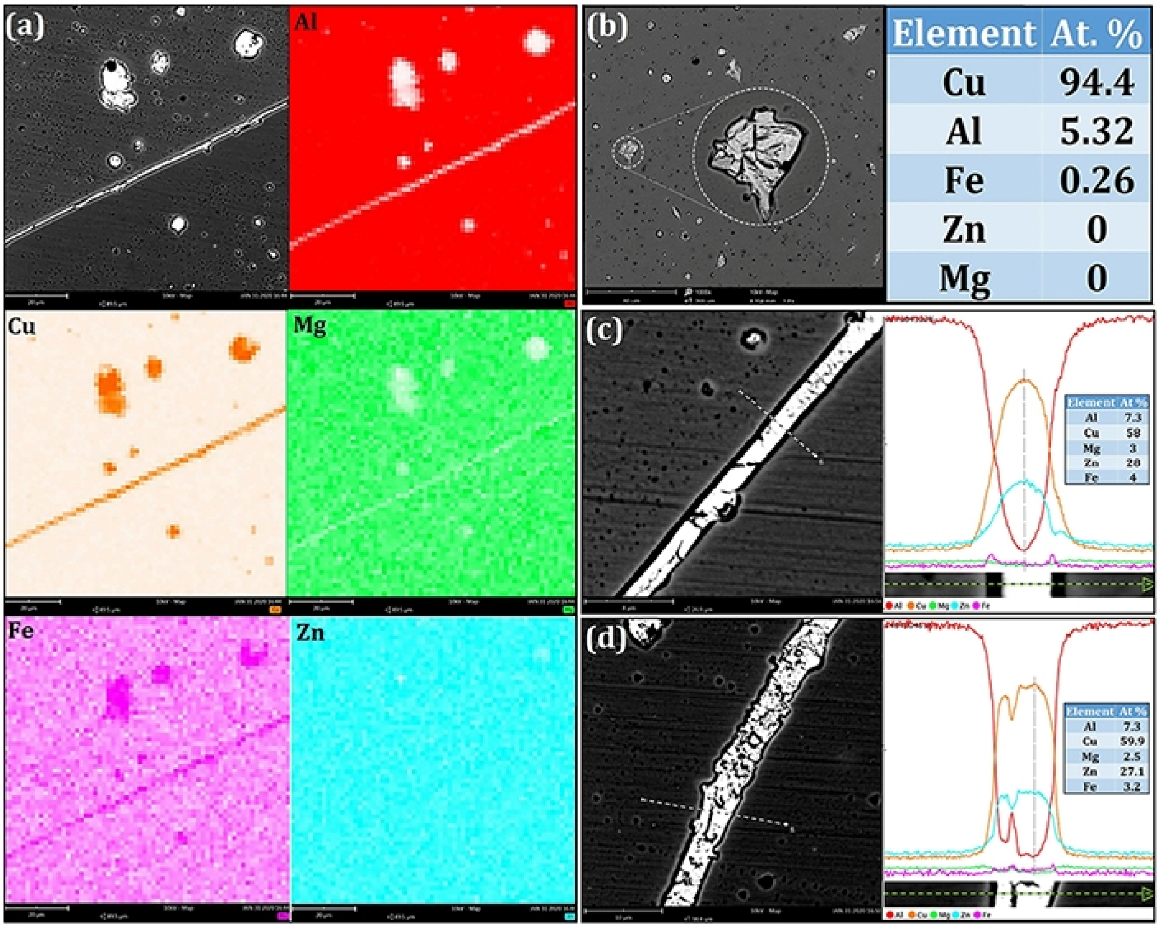

Fig. 3: Results of (a) elemental MAP in AA7475-TMAZ, (b) microchemical analysis of the Cu-rich particles in the SZ adjacent to AA7475, and (c, d) line-scan of the GB phase at AA7475-TMAZ.

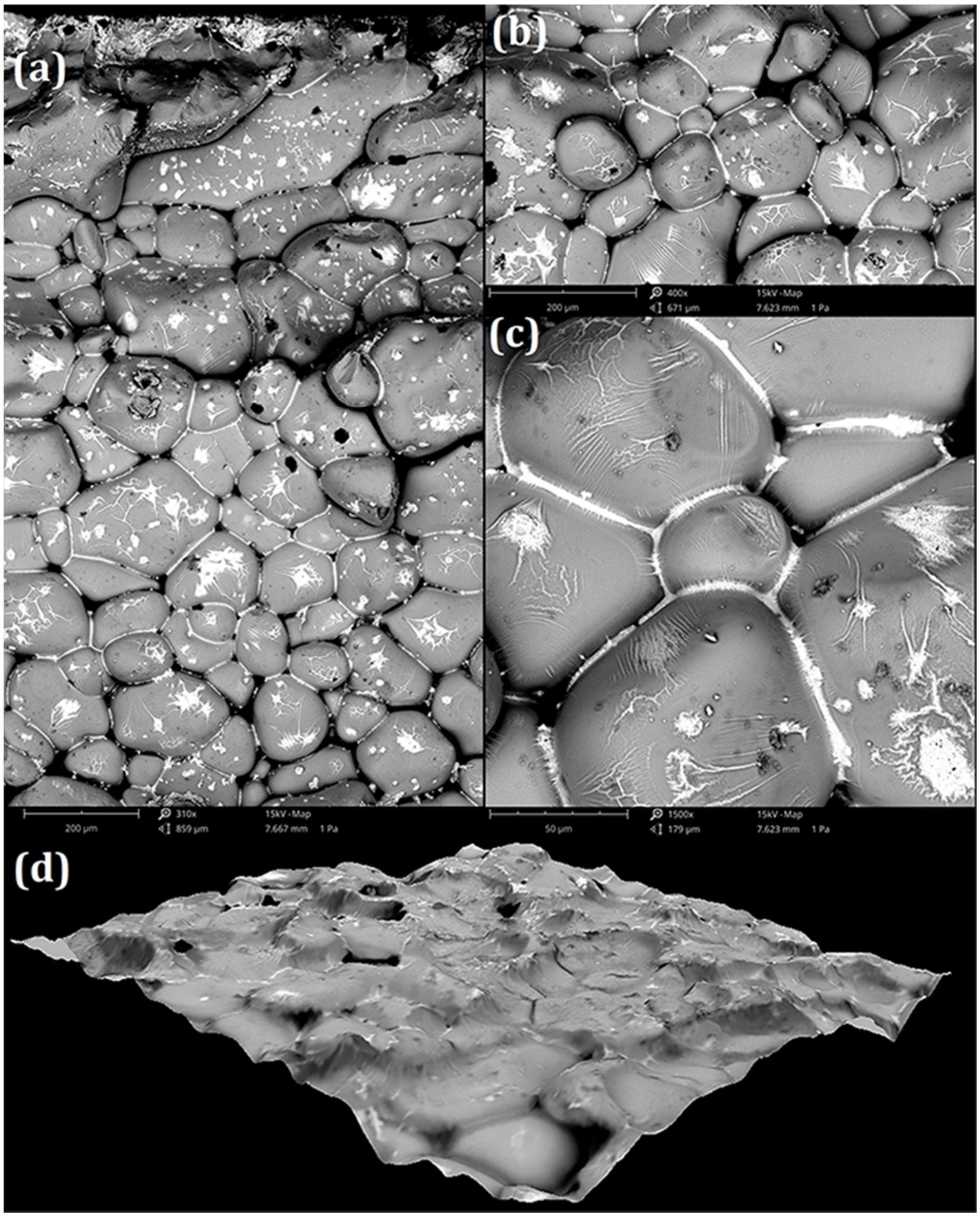

Fig. 4: (a-c) SEM micrographs illustrating the morphology of TMAZ/SZ failure surface, and (d) 3D image showing the topography of the failure surface.